Journal of Engineering Mathematics **42:** 255–264, 2002.

A comparison of linear and nonlinear computations of waves made by slender submerged bodies

E.O. TUCK* and D.C. SCULLEN
*Applied Mathematics Department, The University of Adelaide, SA 5005, Australia *(e-mail: etuck@maths.adelaide.edu.au)*

Received 25 September 2001; Accepted in revised form 22 January 2002

Abstract. Potential flow about a slender spheroid beneath a free surface is considered in order to determine the ability of thin-ship theory to reproduce the free-surface elevation accurately. A fully nonlinear code involving interior Rankine sources is used, enabling comparisons between exact ('Neumann-Stokes') outputs, outputs with exact body condition but linearised free-surface conditions ('Neumann-Kelvin'), and a consistent thin-ship approximation ('Michell-Kelvin'). In general, these computations agree to within a few percent, except when the body is so close to the free surface that the nonlinear computation suggests that breaking is imminent at one point above the body, and even then thin-ship theory still compares well except very near to that isolated point. The thin-ship theory has also been implemented in a separate general-purpose code using Havelock sources, and detailed free-surface contours computed by this linear method are shown for spheroids that are too close to the surface for the nonlinear code to converge.

Key words: free-surface waves, Michell, Neumann–Kelvin, nonlinear, submerged bodies.

1. Introduction

This investigation is intended to provide quantitative information on the extent to which thin-ship theory is a good approximation for computation of free-surface waves made by steadily moving bodies. In order to be definite, we restrict attention in this comparison to a submerged spheroid with a beam-to-length ratio of 0·1. Submerged spheroids have often been used as test cases for ship-wave studies, *e.g.* [1], and the present paper adds some new computations and insights on actual near-field wave elevations. Formally, thin-ship theory *e.g.* [2], [3, p. 572] only requires small beam-to-length ratio, the beam-to-draft ratio being irrelevant, so it should be applicable to such a body. Figure 1 shows the free surface produced by such a submerged body, in the form of detailed contours computed by a thin-ship program SWPE to be described later.

There are two mathematical simplifications that are made by thin-ship theory. The major simplification is that which is common to all linear theories, namely that the kinematic and dynamic free-surface boundary conditions can be approximated by a linearised condition on the plane equilibrium surface. The second simplification is that the disturbance due to the body can be approximated by a (known) continuous distribution of singularities along the centre-plane of the thin body. To gain a better understanding of the influence that these two distinct but connected simplifications have on the accuracy of the approximation, it is necessary to consider their numerical consequences separately. In order to do this, an interior discrete Rankine-source code [4] which is capable of, reproducing all of these different combinations of approximations will be used.

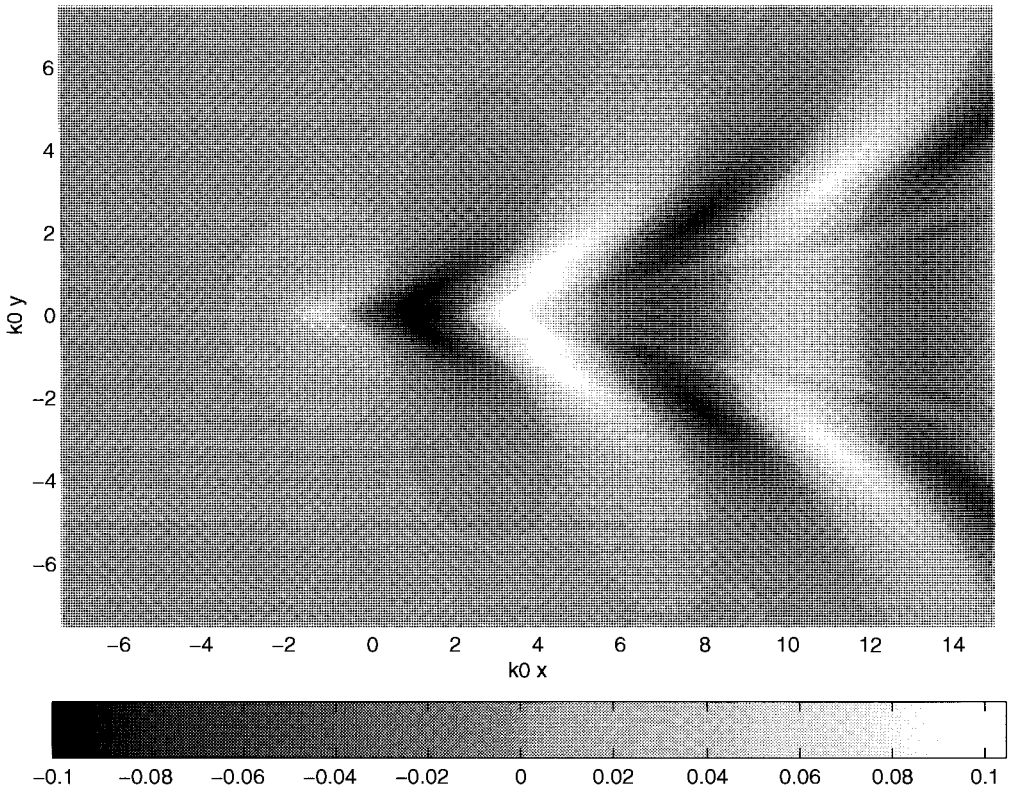

Figure 1. Contour plot of surface elevations due to a spheroid at Froude number 0·5 with diameter-to-submergence ratio 1·5.

Three implementations of the code will be used. The most accurate Neumann–Stokes or 'exact' mode enforces the exact (Neumann) boundary condition on the body, and both the kinematic and dynamic exact (Stokes) boundary conditions on the actual displaced free surface. The Neumann–Kelvin mode (as used in many previous studies: such as [5], [6]) also enforces the exact boundary condition on the body, but approximates the free surface by enforcing only a linearised (Kelvin) boundary condition on the plane $z = 0$. Finally, the Michell–Kelvin or 'thin-ship' mode uses the linearised free-surface condition, and in addition approximates the body boundary condition by use of a continuous distribution of singularities of predetermined (Michell) magnitude along the centre-plane.

The assumption will then be made that the Neumann–Stokes mode renders (of these three modes) the best approximation to the (unknown) exact solution, and therefore this output will be used as the benchmark for accuracy comparisons, especially to assess the accuracy of the Michell–Kelvin or thin-ship theory. This comparison thus concentrates on errors in the thin-ship assumption, as distinct from errors associated with the physical model, such as neglect of viscosity.

Two free-surface error measures are used, one of which identifies maximum errors, occurring at the highest crests and lowest troughs in the wave field. Such local isolated errors in thin-ship theory can be as high as 50% for the most shallow submergences used here, where the largest waves are very near to breaking. However, the general magnitude of the error over the whole wave field is even then only of the order of 5% or less, and this is displayed by use of a root-mean-square error estimate, averaging errors over the whole field.

As the submergence is increased, the thin-ship error reduces dramatically, but not to zero. There is still a small (2% to 3%) residual error even at large submergences, attributable to the inability of the Michell body boundary condition to capture the true local flow around the nose and tail of bluff bodies such as spheroids, and this residual error can only be reduced by reverting to the exact Neumann body boundary condition. However, it is swamped by a much larger error due to the Kelvin free-surface approximation when the body is close to the free surface.

2. Exact and approximate boundary conditions

Our task (assuming steady irrotational flow of an inviscid incompressible fluid of infinite depth) is to solve Laplace's equation

$$\phi_{xx} + \phi_{yy} + \phi_{zz} = 0 \tag{1}$$

for the disturbance potential $\phi(x, y, z)$ to a stream U due to the presence of a body $y = \pm Y(x, z)$, beneath a free surface $z = Z(x, y)$. The exact Neumann body boundary condition is

$$\phi_y = \left[U + \phi_z\right] Y_x + \phi_z Y_z \quad \text{on} \quad y = Y(x, z), \tag{2}$$

and the exact Stokes free-surface conditions (on the unknown free-surface $z = Z$) are

$$\phi_z = \left[U + \phi_x\right] Z_x + \phi_y Z_y \tag{3}$$

and

$$gZ + \tfrac{1}{2}\left[(U + \phi_x)^2 + \phi_y^2 + \phi_z^2\right] = \tfrac{1}{2}U^2. \tag{4}$$

We are interested in thin bodies with small Y and hence small ϕ and Z. In that case, the Neumann condition (2) is approximated by the Michell condition

$$\phi_y = U Y_x \quad \text{on} \quad y = 0_+, \tag{5}$$

and the Stokes boundary conditions (3, 4) by approximations which may be combined to give the Kelvin condition

$$g\phi_z + U^2\phi_{xx} = 0 \quad \text{on} \quad z = 0. \tag{6}$$

Although it is consistent to make both the Michell and Kelvin approximations together (since both are ultimately due to smallness of Y), it is our present aim to consider their effects separately.

3. Brief description of the numerical method

The Rankine source program, in its most accurate (Neumann–Stokes) mode, solves (1) subject to the boundary conditions (3, 4), and is fully described in [4]. The velocity potential $\phi(x, y, z)$ is represented by the sum of a finite but large number of discrete Rankine sources distributed externally to the fluid domain (that is, both inside the body and above the free surface). An iterative procedure is employed to refine successively approximations to the free surface and

potential (via the unknown source strengths) until an accurate solution is obtained. Considerable care is taken when developing the iterative procedure (as in [7]) to ensure a quadratic rate of convergence to the desired solution.

It was found that the program was more robust if the kinematic condition (3) was replaced by a condition that the pressure remained constant when following a fluid particle. A radiation condition was enforced numerically to eliminate waves far ahead of the body. The Rankine source strengths are all unknown in advance, and are determined as part of the solution process. Their positions are fixed during the iteration, those inside the body at a pre-determined distance inside the hull, and those above the free surface at a pre-determined distance above the plane $z = 0$.

For the linear modes of the program, when the Kelvin free-surface condition (6) is used, iteration is not required, and the source strengths are determined by solving linear algebraic equations once only. For the Neumann–Kelvin problem, Rankine sources are still placed at fixed distances inside the actual hull surface, but for the Michell–Kelvin problem the interior singularities are replaced by centreplane distributions of horizontal dipoles of known strength.

An advantage of locating singularities externally to the fluid domain is that the potential and its derivatives can be evaluated easily everywhere on the boundaries. This also allows greater freedom when choosing their locations and, with care, they may be located so that the boundary conditions are satisfied not only at the discrete collocation points at which the boundary conditions are exactly enforced, but also (to at least 4-figure accuracy) on the boundary segments that join them, thus producing a significantly more accurate representation of the body than might otherwise be the case. Another advantage of Rankine sources and dipoles is that their potential and derivatives are straightforward and inexpensive to compute.

4. Representation of body and free surface

Firstly, an accurate representation of the flow about a spheroid is sought, such that the flux through the body's surface is minimal. On the basis of an investigation of equivalent deeply-submerged flows, we chose to use 65 stations, each having 32 nodes equally spaced in angle around the circumference of the circular cross-section, although symmetry means that there are only 17 unknown source strengths per station, thus about 1100 unknowns attributable to the body.

Similarly, a representation of the free surface which simultaneously satisfies several criteria is sought. The free-surface domain must extend far enough downstream to capture several wavelengths, far enough upstream to implement a radiation condition, be large enough to represent the flow around the body, have fine enough resolution to resolve both the free-surface waves and the body, and be comprised of few enough collocation points to be computationally feasible. Needless to say, it is not always possible to satisfy all of the criteria given current super-computing capabilities, especially at the highest and lowest Froude numbers of interest. Nevertheless, a representation which uses 91 collocation points in the x-direction, 49 collocation points in the y-direction and extends from $x = -3{\cdot}75U\sqrt{L/g}$ to $7{\cdot}5U\sqrt{L/g}$ proves to be adequate over the range of Froude numbers that are considered here. Thus (again using y-symmetry) we have about 2300 unknowns attributable to the free surface, making a total of about 3400.

When using the program in the thin-ship mode, we observe that the Michell boundary condition (5) is satisfied by using a centreplane distribution of x-directed dipoles, of moment

proportional to the local body thickness $2Y(x, z)$. For numerical purposes we approximate this known continuous distribution by a collection of discrete dipoles, with strengths weighted by the area that they represent. The centreplane ellipse is discretised in the x-direction into 65 strips, each of which is further discretised in the z-direction into 17 rectangular cells, so maintaining consistency with the number of Rankine sources used to satisfy the Neumann boundary condition.

5. Error measures

Comparisons between free surfaces produced by the various modes of computation are made for the 1:10 spheroid, for various diameter-to-submergence ratios and Froude numbers. We calculated error measures using the (exact) Neumann–Stokes mode as the benchmark for the comparison. In particular, a scaled maximum error and a scaled root-mean-square (r.m.s.) error are determined as follows. The scale used for this comparison is determined by the exact solution, namely the vertical distance H between the lowest trough and the highest crest in the whole wave field.

Then, at each point on the free surface, we determine the difference between the approximate and exact elevations $Z(x, y)$. The maximum error is then defined as the difference between the (positive) maximum and (negative) minimum values of this difference, and the scaled maximum error is the ratio between that maximum error and the scale H. In a similar manner, we can determine the mean square error in the free surface by averaging the square of the point-wise elevation differences over the whole field, and divide the square root of this quantity by H to give the scaled r.m.s. error.

The maximum error tends to overstate the discrepancies at points of the surface other than that where the maximum error occurs. It is entirely determined by the error that occurs near the very highest crest and deepest trough in the wave field (usually in the near field close to the stern), and this particular wave element can be close to or actually breaking when the body is shallowly submerged. It is difficult for any numerical code to estimate such near-breaking waves, and differences between various approximation methods, including the Neumann–Kelvin and Michell–Kelvin modes tested here, become exaggerated. Meanwhile, however, at points other than the extreme crests and troughs, the errors are far less at the same speeds and submergences.

This is accounted for in part by the r.m.s. error, which averages errors over the whole flow field. On the other hand, the r.m.s. error somewhat understates the magnitude of the error, since for example a significant part of the domain where computations are being compared lies upstream of the wake, where all disturbances are small and hence only small contributions are made to the average. However, a combination of these two measures of the error can be useful to judge the accuracy of the results.

6. Accuracy comparisons

Figure 2 shows the scaled maximum error of the Michell–Kelvin thin-ship mode for various Froude numbers and diameter-to-submergence ratios, while Figure 3 similarly shows the scaled r.m.s. error. The diameter-to-submergence ratio increases in steps of 0·1, from 0·1 at the bottom to 1·0 at the top, in this and all other curves in this series. That is, the bottom curve

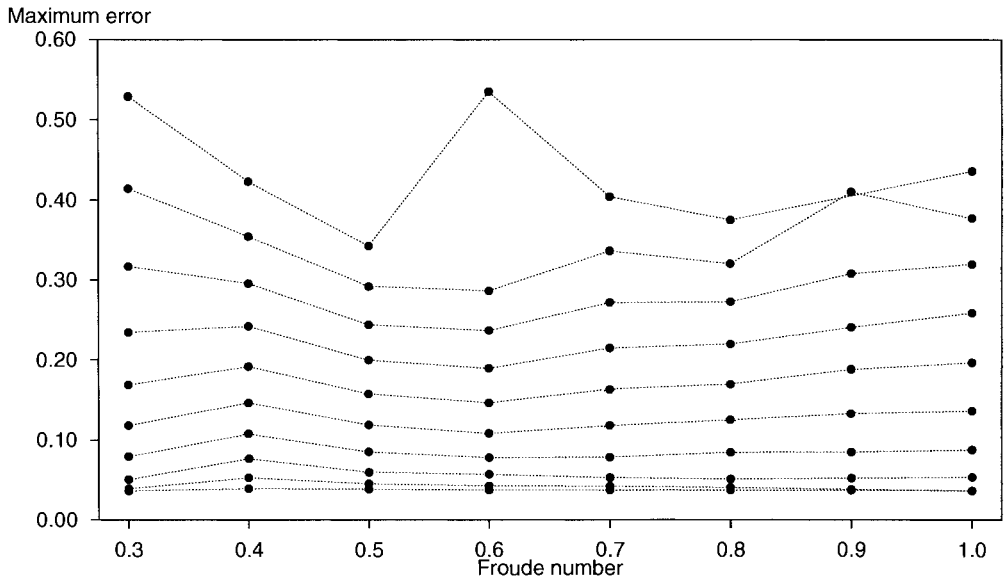

Figure 2. Scaled maximum error in the free surface computed by the thin-ship mode when compared to that computed by the exact mode for the 1:10 spheroid. In this and other figures to follow the diameter-to-submergence ratio increases in steps of 0·1, from 0·1 to 1·0 from bottom curve to top curve.

is for the largest submergence, with little disturbance to the free surface, whereas the top curve is for the most shallowly submerged case, where the highest waves are made.

The most shallow submergence tested, with diameter-to-submergence ratio 1·0, corresponds to a half-diameter of water above the highest point of the hull. The maximum error is then quite large, of the order of 50% or more, but the wave front between, the deepest trough and the highest crest is so steep that it is on the verge of breaking and is inevitably poorly predicted by the linear theory.

On the other hand, the bottom curve in the figure, with diameter-to-submergence ratio 0·1, corresponding to deeply submerged bodies, has maximum errors of the order of 4% or less, because the waves are smaller and more easily predicted by linear theory. Meanwhile, the r.m.s. error as displayed in Figure 3 is consistently much lower than the maximum error, of the order of 5% for shallowly-submerged bodies at low Froude number, reducing to the order of 2% or less for all submergences at high Froude number.

These two figures give an indication of the total error that is to be expected when approximating this nonlinear wave-generation problem by a consistent linearised formulation. Of particular interest is the fact that the errors tend to a non-zero minimum as the diameter-to-submergence ratio is decreased; that is, as the body becomes more and more deeply submerged. This indicates that there is a residual error associated with the Michell approximation to the body boundary condition, independent of the presence of the free surface.

It is of interest to repeat these comparisons, again using the exact Neumann–Stokes mode as the basis for the comparison, but this time using the Neumann–Kelvin mode instead of the Michell-Kelvin results as the approximation, *i.e.* to assess the effect of the linearised free-surface condition in isolation.

Figures 4 and 5 show the resulting scaled maximum errors and r.m.s. errors. For the mid-to-high Froude numbers, the maximum errors for shallowly submerged bodies (in the top curves for which the diameter-to-depth ratio is 1·0) remain essentially the same as for the Michell–

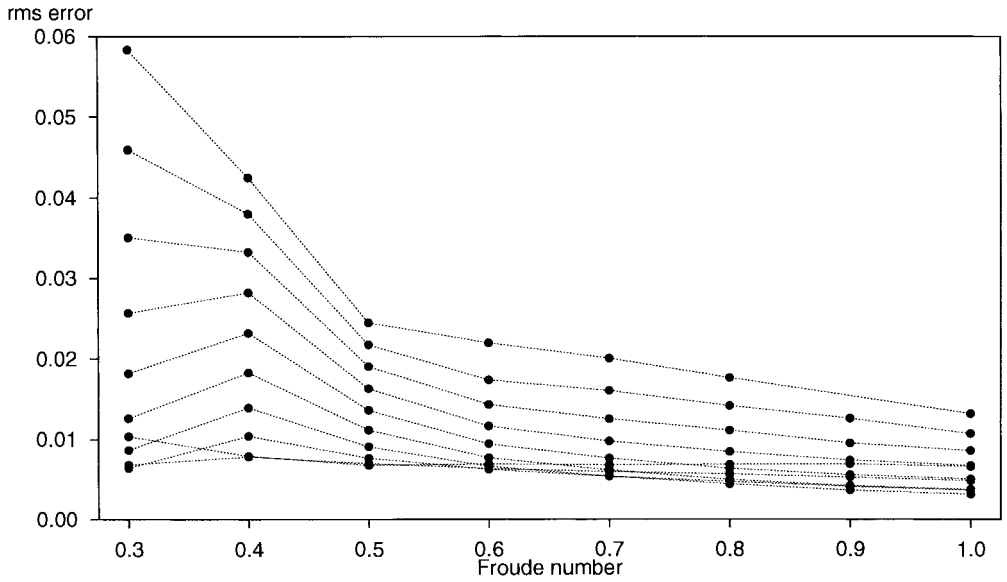

Figure 3. Scaled r.m.s. error in the free surface computed by the thin-ship mode when compared to that computed by the exact mode for the 1:10 spheroid.

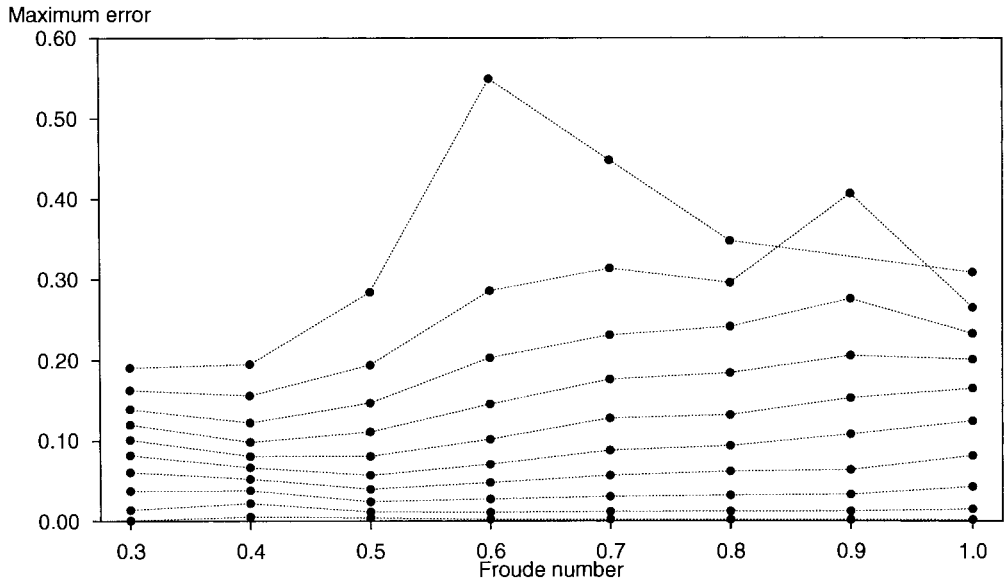

Figure 4. Scaled maximum errors in the free surface when Neumann–Kelvin results are compared to Neumann–Stokes results for the 1:10 spheroid.

Kelvin approximation, indicating that nonlinear free-surface effects account for much (but not quite all) of this error. On the other hand, for smaller Froude numbers, the errors are now significantly reduced, indicating that the body boundary condition is more important then.

Also, one can see that the error now tends to zero as the diameter-to-submergence ratio approaches zero. The residual errors of the order of 3% for deeply-submerged bodies when in Michell–Kelvin mode are thus due to the inability of the distribution of singularities along the centre-plane to reproduce the flow about the body in an accurate manner. Such errors (of the

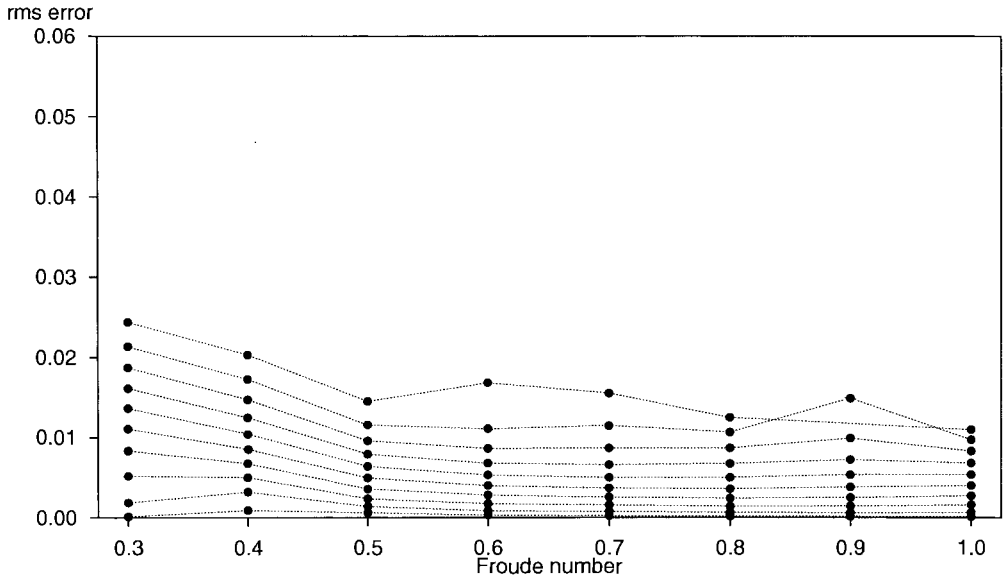

Figure 5. Scaled r.m.s. errors in the free surface when Neumann–Kelvin results are compared to Neumann–Stokes results for the 1:10 spheroid.

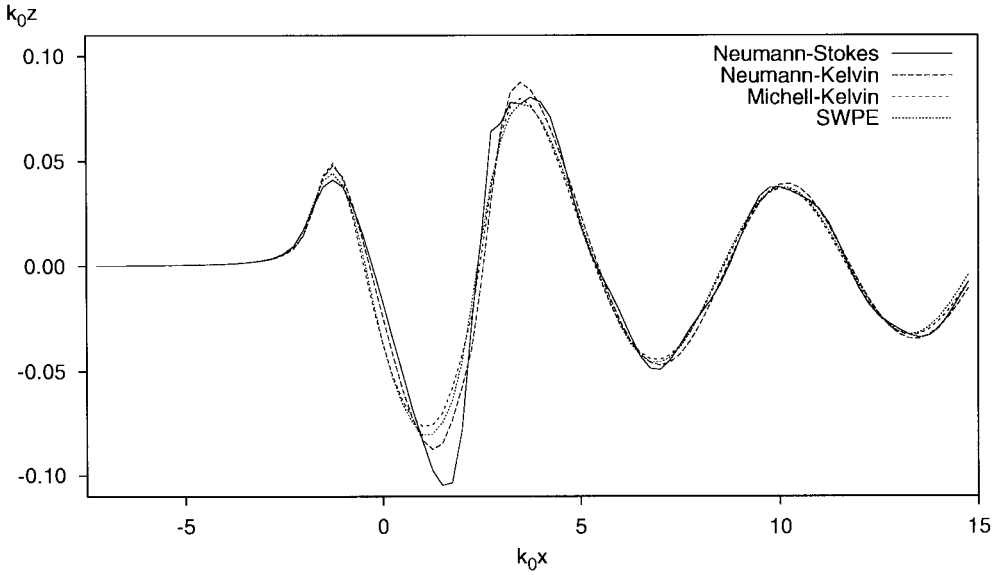

Figure 6. Centreline surface elevations for all three modes of the Rankine-source code and SWPE for a spheroid with Froude number 0·5 and diameter-to-submergence ratio 1·0. The spheroid extends from bow at $k_0x = -2{\cdot}0$ to stern at $k_0x = +2{\cdot}0$.

order of a maximum of 3% for beam-to-length ratio 0·1, and varying in proportion to beam-to-length ratio) will be present at all depths, though overwhelmed by larger free-surface errors for shallow submergences.

As an aside, one should note that the effects of the two approximations are not simply additive. That is, one cannot simply take the error due to nonlinearity and add it to the error due to the body representation, and arrive at the error in the consistent thin-ship approximation.

The conclusion that the body-boundary-condition approximation produces a residual error at large submergence is supported further when we analyse the wave resistance produced by the various modes, again using the nonlinear results as the basis for comparison. Although we do not show the results here, we then see a similar pattern, with the relative error in the Neumann–Kelvin wave resistance tending to zero as the submergence is increased, whereas the relative error in the Michell–Kelvin wave resistance (which is Michell's original [2] integral) tends to a non-zero limit. For the 1:10 spheroid, this limiting relative error in the wave resistance is approximately 6%.

7. Thin-ship results via Havelock sources

In the above comparison study for the submerged spheroid, the code always used Rankine sources, and hence these sources needed to be placed both inside the body and above the free surface. For any linearised problem, where the Kelvin free-surface condition is being used, it is more efficient for highly detailed computations to use 'Havelock' sources which satisfy the Kelvin condition exactly, so that sources are only needed inside the body. A Havelock source located at $(x, y, z) = (0, 0, \zeta)$ is defined ([3, p. 484]) by

$$G(x, y, z; \zeta) = -\frac{1}{4\pi r} + \frac{1}{4\pi^2}\Re\mathfrak{e}\int_{\pi/2}^{\pi/2} \mathrm{d}\theta \int_0^\infty \mathrm{d}k \frac{k + k_0 \sec^2\theta}{k - k_0 \sec^2\theta}\, e^{\mathrm{i}k(x\cos\theta + y\sin\theta) + k(z+\zeta)}, \tag{7}$$

where $r = \sqrt{x^2 + y^2 + (z-\zeta)^2}$ and the path of k-integration passes above the pole at $k = k_0 \sec^2\theta$, with $k_0 = g/U^2$. The first term is the ordinary infinite-fluid Rankine source, and the double integral is the correction for the free surface. The Michell–Kelvin solution is then a distribution of such sources, of strength $2UY_x$ per unit area, over the centreplane R, *i.e.*

$$\phi(x, y, z) = 2U \iint_R Y_\xi(\xi, \zeta) G(x - \xi, y, z; \zeta)\, \mathrm{d}\xi\, \mathrm{d}\zeta. \tag{8}$$

We have developed code to compute the Michell–Kelvin solution for the wave elevation $z = Z(x, y) = -(U/g)\phi_x(x, y, 0)$ in the form

$$Z(x, y) = \frac{1}{\pi^2}\Re\mathfrak{e}\int_{\pi/2}^{\pi/2} \mathrm{d}\theta \int_0^\infty \mathrm{d}k \frac{k^2}{k - k_0 \sec^2\theta}(P + \mathrm{i}Q)\, e^{\mathrm{i}k(x\cos\theta + y\sin\theta)} \tag{9}$$

where

$$P + \mathrm{i}Q = \iint_R Y(x, z)\, \mathrm{e}^{\mathrm{i}k\cos\theta x + kz}\mathrm{d}x\, \mathrm{d}z. \tag{10}$$

This code 'SWPE' is described in [8]. Results from SWPE for submerged spheroids agree closely with those computed using the Michell–Kelvin mode of the Rankine-source code, but have the advantage that a very finely detailed free surface of more than 100,000 points can be computed very rapidly.

Figure 6 shows the centreline free-surface elevations produced by all three modes of the Rankine-source code and by SWPE. The particular case shown is that of a 1:10 spheroid at Froude number $F = 0{\cdot}5$ with diameter-to-submergence ratio of $1{\cdot}0$. In the figure, all lengths

have been scaled by k_0, so the spheroid has length 4 and diameter 0·4, and is located with its centre directly beneath the origin and at depth 0·4.

In general, all four results are very similar, with differences between the results becoming apparent only in the immediate neighbourhood of the body. The dominant nonlinear feature is the deepening of the primary trough near the stern (the free surface there being sucked down due to reduced pressure as the fluid accelerates past the spheroid) and a consequent increase in steepness of the following wave face. Thus for this test case at least (see [9] for some other similar tests), any of the linearised approximations gives an accurate representation of the free surface, and in particular the thin-ship approximation is very satisfactory.

Figure 1 shown earlier demonstrates the ability of the Havelock-source code SWPE to determine very detailed free-surface contours near a spheroid submerged to a depth less than that which is possible using the fully-nonlinear code. Here we keep the Froude number at $F = 0{\cdot}5$, but increase the diameter-to-submergence ratio to 1·5, so that, the spheroid is now centred at a depth of 0·267, with only 0·067 units of water above it when at rest. In fact the spheroid is now so shallowly submerged that SWPE predicts that it is partially exposed at the primary trough when in motion. A clear advantage of the thin-ship theory in this case is the ability to robustly produce free-surface elevations, even when in reality there may be a highly-localised breaking wave, and when any sufficiently accurate nonlinear code must fail to converge for this reason.

References

1. V. Bertram, W.W. Schultz, Y. Cao and R.F. Beck, Nonlinear computations for wave drag, lift and moment of a submerged spheroid. *Schiffstechnik* 38 (1991) 3–5.
2. J.H Michell, The wave resistance of a ship. *Phil. Mag.* 5th series 45 (1898) 106–123.
3. J.V. Wehausen and E.V. Laitone, Surface waves. In: S. Flügge (ed.), *Handbuch der Physik*, vol. 9. Berlin: Springer-Verlag (1962) pp. 446–778.
4. D.C. Scullen, *Accurate Computation of Steady Nonlinear Free-Surface Flows*. Ph.D. thesis, Department of Applied Mathematics, The University of Adelaide, February 1998. (downloadable from http://www.maths.adelaide.edu.au/Applied/staff/dscullen/Web_pages/publications.html).
5. L.J. Doctors and R.F. Beck, Numerical aspects of the Neumann–Kelvin problem. *J. Ship Res.* 31 (1987) 1–13.
6. R. Brard, The representation of a given ship form by singularity distributions when the boundary condition on the free surface is linearized. *J. Ship Res.* 16 (1972) 79–92.
7. D.C. Scullen and E.O. Tuck, Nonlinear free-surface flow computations for submerged cylinders. *J. Ship Res.* 39 (1995) 185–193.
8. E.O. Tuck, D.C. Scullen and L. Lazauskas, Ship-wave patterns in the spirit of Michell. In: A.C. King and Y.D. Shikhmurzaev (eds.), IUTAM Symposium on Free-Surface Flows. Dordrecht, The Netherlands: Kluwer Academic Publishers (2001) pp. 311–318.
9. Y. Cao, W.W. Schultz and R.F. Beck, Three-dimensional desingularized boundary integral methods for potential problems. *Int. J. Num. Meth. Fluids* 11 (1990) 785–803.